



Photocatalytic and antimicrobial activities of $\text{Sr}_x\text{Ca}_{(1-x)}\text{TiO}_3$ ($x=0, 0.25, 0.5, 0.75$ and 1) powders synthesized by solution combustion technique

Oratai JONGPRATEEP^{1,2}, Nicha SATO^{1,*}, Ratchatee TECHAPIESANCHAROENKIJ^{1,2}, Krissada SURAWATHANAWISES¹, Patcharaporn SIWAYAPRAHM³, and Phonphan WATTHANARAT³

¹ Department of Materials Engineering, Faculty of Engineering, Kasetsart University, Bangkok, 10900, Thailand

² Materials Innovation Center, Faculty of Engineering, Kasetsart University, Bangkok, 10900, Thailand

³ Department of Microbiology, Faculty of Science, Kasetsart University, Bangkok, 10900 Thailand

*Corresponding author e-mail: nicha.sat@ku.ac.th

Received date:
29 September 2018
Revised date:
29 November 2018
Accepted date:
19 December 2018

Keywords:
Strontium calcium titanate
Doping
Photocatalytic activity
Solution combustion synthesis
Antibacterial

Abstract

Unique dielectric properties of strontium titanate and calcium titanate accommodate utilization of the materials in electronic devices. Doping generally alters microstructure and electronic band structure, which influence catalytic performance of the materials. This study aimed at examining photocatalytic activities of $\text{Sr}_x\text{Ca}_{(1-x)}\text{TiO}_3$ ($x = 0, 0.25, 0.5, 0.75$ and 1) powders synthesized by solution combustion technique. Relationships among chemical composition, microstructure, bandgap, photocatalytic and antimicrobial performance of $\text{Sr}_x\text{Ca}_{(1-x)}\text{TiO}_3$ were also examined. Experimental results revealed that according to the initial compositions single phases of CaTiO_3 , $\text{Sr}_x\text{Ca}_{(1-x)}\text{TiO}_3$ and SrTiO_3 were observed. Sub-micrometer-sized particles, with average specific surface area ranging from 4.2 to $7.4 \text{ m}^2 \cdot \text{g}^{-1}$, were present. Reduction of bandgap energy was evident in the $\text{Sr}_x\text{Ca}_{(1-x)}\text{TiO}_3$ ($x = 0.25, 0.5,$ and 0.75) powders. Attributed to superior specific surface area and minimal bandgap energy, the greatest photocatalytic degradation of methylene blue measured at wavelength close to 660 nm was observed in $\text{Sr}_{0.75}\text{Ca}_{0.25}\text{TiO}_3$. Experimental results also revealed decent antibacterial performance with percent of bacterial colony reduction greater than 90% . The antibacterial results agreed well with the photocatalytic performance.

1. Introduction

Attributed to their relatively narrow bandgap, metal oxides such as TiO_2 , ZnO , CeO_2 , SnO_2 and ZnO , are widely recognized as prominent photocatalysts exploited in applications involving waste water treatment and antimicrobial activities [1-3]. On the contrary, perovskite-structured materials such as CaTiO_3 , SrTiO_3 and BaTiO_3 have relatively wide bandgaps and exhibit spontaneous polarization. Hence, the perovskite titanates are primarily recognized as dielectric materials used in fabrication of capacitors [4-5].

Despite relatively wide bandgap, the perovskite titanates are capable to being utilized in photocatalytic applications. With the unique properties such as photostability, and resistance to photocorrosion in solution, the materials demonstrate their good potential as photocatalysts [6-7]. Additionally, owing to structural stability, electron-hole recombinations in the perovskite materials are considered low compared with that of TiO_2 . With the low carrier recombination, photocatalytic performance can be enhanced [8-10].

To enhance photocatalytic properties, doping can be used to promote a generation of reactive electrons through reduction of bandgap energy [11]. Tailoring bandgap energy in the perovskite titanates by doping can also be achieved. Narrower bandgap has been reported in La-doped BiTiO_3 , Mn/Fe/Co-doped

SrTiO_3 , and Ag/La-doped CaTiO_3 compared with the undoped ones [12-14]. It has also been reported that a lattice distortion caused by doping results in an increase in photogenerated charge carriers, which consequently accommodate redox reactions in the photocatalysis process [15].

Decent photocatalytic performances of perovskite titanates have been reported. According to Tubchareon et al. [16], metal doping in A site of the perovskite-structured barium strontium titanate demonstrated high photocatalytic activity and dye degradation. Degradation of rhodamine B, methylene blue and methyl orange as high as 40% could be achieved in strontium titanate, according to da Silva et al. [17]. Calcium titanate was also reported to perform degradation of methylene blue as well as antimicrobial activity [18,19].

Mechanisms related to photocatalytic activity involve excitation of the photocatalyst by photon with sufficient energy. Electrons are excited and jump from valence band to conduction band, leaving holes within the valence band. While electrons react with oxygen and create super oxide (O_2^-), holes oxidize with hydroxide, water or other reactive species, forming hydroxyl radical (OH^\bullet), perhydroxyl radical (HO_2^\bullet) or hydrogen peroxide (H_2O_2). Photocatalytic reactions of calcium titanate can be expressed by the following expression [20]:



To further improve photocatalytic performance of the particulate photocatalysts, specific surface enhancement as well as compositional control of the materials should be conducted [21]. Numerous techniques are exploited as methods to synthesize particles with high specific surface area. Solution combustion technique, a simple, rapid and cost-effective technique capable of producing fine ceramic powders with chemical homogeneity, was selected as the powder preparation technique in this study.

This study aimed at examining photocatalytic activities and potential application of $Sr_xCa_{(1-x)}TiO_3$ ($x = 0, 0.25, 0.5, 0.75$ and 1) powders synthesized by solution combustion technique. Relationships among chemical composition, microstructure, bandgap, photocatalytic and antimicrobial performance of $Sr_xCa_{(1-x)}TiO_3$ were also examined.

2. Experimental

Strontium calcium titanate with the composition $Sr_xCa_{(1-x)}TiO_3$, where $x=0, 0.25, 0.5, 0.75$ and 1 , was synthesized by solution combustion technique. The preparation process consisted of 0.54 M aqueous solution containing oxidizers and fuel. Strontium nitrate ($Sr(NO_3)_2$, Daejung), calcium nitrate ($Ca(NO_3)_2$, Daejung) and titanium dioxide (TiO_2 , Sigma-Aldrich) dispersed in nitric acid (HNO_3 70%, Univar) were used as oxidizers, whereas glycine acted as combustion fuel during the combustion. To initiate the combustion reaction, the solution containing oxidizer and fuel were heated on a hotplate at the temperature close to $400^\circ C$. The powders obtained from the combustion reaction were subsequently calcined at $900^\circ C$ for 3 h [22].

The powders were compositionally and microstructurally examined by an x-ray diffractometer (Philips, X'Pert) and a scanning electron microscope (Phillip, XL30), respectively. Diffraction patterns were obtained over angles ranging from 35° to 75° in 2θ , at a step size of 0.02° and a scan rate of 0.7 seconds/step. Image J software was employed in analysis of micrographs and in determination of cluster sizes of the powders. Brunauer-Emmett-Teller (BET) technique (Micrometrics, 3Flex) was employed in obtain information related to specific surface area of the powders.

Bandgap energies, photocatalytic activities and anti-microbial performance of the powders were also examined. Absorption of light, measured by a UV-Vis spectrophotometer (UV-1700) at the wavelength ranging from 300 to 900 nm, was utilized in determination of optical bandgap energy, according to the following equation:

$$(ah\nu)^2 = h\nu - E_g \quad (2)$$

where α is the absorption coefficient, E_g is the bandgap energy (eV), h is the Planck's constant (Js) and ν is the wave frequency.

Decomposition of methylene blue was used as an indicator of photocatalytic performance of the powders. The synthesized powders were dispersed in 5 ppm methylene blue ($C_{16}H_{18}ClN_3S$, Daejung) and placed in the QUV accelerated weathering apparatus (Q-Lab) under the following conditions: 0.44 Wm^{-2} at $50^\circ C$. Absorbance and transmittance of the prepared solutions were recorded. Decomposition of methylene blue was conducted at 60 and 90 min using absorbance results from the UV-Vis spectrophotometer. Percent of methylene blue degradation was determined from the absorbance, using the following equations:

$$\% \text{ Degradation} = \left(\frac{A_0 - A_t}{A_0} \right) \times 100 \quad (3)$$

where A_0 is the absorbance at time $t = 0$ min and A_t is the absorbance at $t = 60$ and 90 min after decomposition.

In-vitro evaluation of bacterial activity was conducted using gram-positive *Staphylococcus aureus* (*S. aureus*) strain ATCC6538. Preparation of single bacterial colonies was achieved by streaking bacterial strain into Tryptic Soy Agar (TSA) plate, and incubated at $37^\circ C$ for 24 h. Single colony was picked up and suspended in 0.85% saline solution. Turbidity of the bacterial suspension was adjusted to attain 0.5 McFarland standard (approximately $1.5 \times 10^8 \text{ CFU} \cdot \text{mL}^{-1}$). The cell suspension was then diluted to obtain colony forming of $10^4 \text{ CFU} \cdot \text{mL}^{-1}$. The synthesized $Sr_xCa_{(1-x)}TiO_3$ powder with concentration of 150 ppm was mixed with the TSA medium and autoclaved at $121^\circ C$ for 15 min. The mixture was poured into a sterile petri plate, which was subsequently inoculated by the diluted bacterial suspension. The TSA plate was then incubated at $37^\circ C$ for 24 h, before the number of bacterial colonies were counted and calculated.

3. Results and discussion

3.1 Chemical composition and microstructure

An x-ray diffraction analysis revealed that the synthesized powder with initial composition of $Sr_xCa_{(1-x)}TiO_3$ (where $x = 0$) contained a single phase of calcium titanate ($CaTiO_3$) (JCPDS 082-0230), while the $Sr_xCa_{(1-x)}TiO_3$ (where $x = 1$) contained a single phase of strontium titanate (JCPDS 089-7049, 089-8031), as shown in Figure 1. For the $Sr_xCa_{(1-x)}TiO_3$ (where $x = 0.25, 0.5$, and 0.75), strontium calcium titanate (JCPDS 073-0661) phase was observed. None of the secondary phase was detected. It is noted that the x-ray diffraction patterns of the powders were indistinguishable with those of the powders reported in the dielectric property study, previously reported by Jongprateep et al. [22].

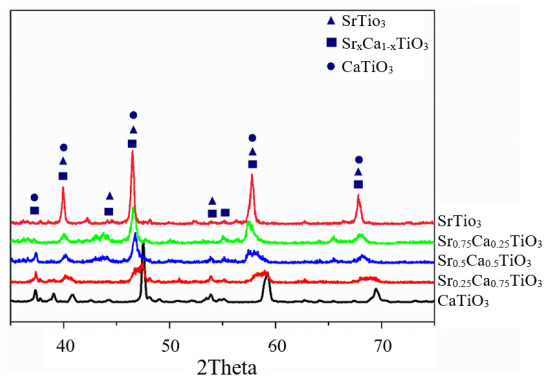


Figure 1. X-ray diffraction pattern of $\text{Sr}_x\text{Ca}_{(1-x)}\text{TiO}_3$, where $x=0, 0.25, 0.5, 0.75$ and 1 powder synthesized by solution combustion technique.

Morphological examination of the synthesized powders revealed fine equi-axial particles with average sizes smaller than $0.4 \mu\text{m}$. The particles, however, agglomerated into irregular-shaped clusters with average sizes ranging from 0.98 ± 0.40 to $1.61 \pm 0.67 \mu\text{m}$, as shown in Figure 2. Specific surface areas of the powders were in the range between 4.2 and $7.4 \text{ m}^2\text{g}^{-1}$, as shown in Table 1. The results from the BET technique and image analysis were being agreed. The powders agglomerated into larger cluster size tended to exhibited smaller specific surface area. The results, however, did not reveal significant effects of strontium concentrations on microstructure and surface area.

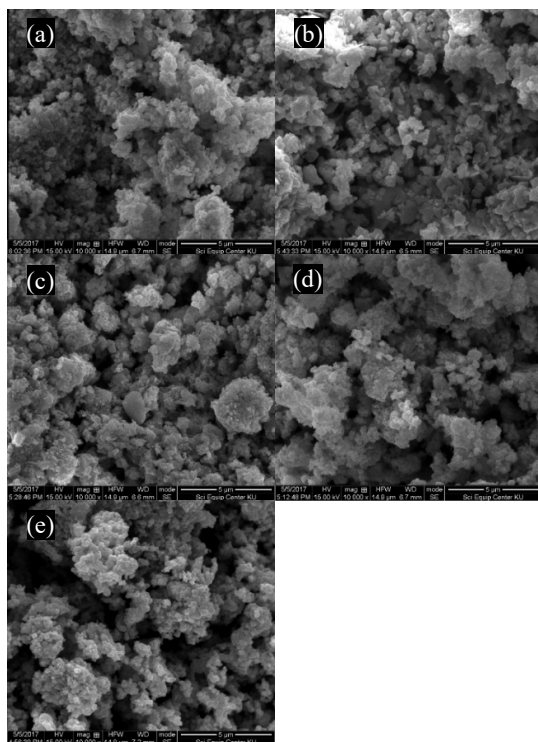


Figure 2. Scanning electron micrographs showing particle morphology of powders prepared by solution

combustion synthesis with following compositions: (a) CaTiO_3 , (b) $\text{Sr}_{0.25}\text{Ca}_{0.75}\text{TiO}_3$, (c) $\text{Sr}_{0.5}\text{Ca}_{0.5}\text{TiO}_3$, (d) $\text{Sr}_{0.75}\text{Ca}_{0.25}\text{TiO}_3$ and (e) SrTiO_3

Table 1. Particle size, cluster size and specific surface area of $\text{Sr}_x\text{Ca}_{(1-x)}\text{TiO}_3$.

Concentration of Sr (at%)	Particle size (μm)	Cluster size (μm)	SSA (m^2g^{-1})
0.00	0.25 ± 0.05	0.98 ± 0.40	5.99
0.25	0.19 ± 0.06	1.40 ± 0.58	7.43
0.5	0.25 ± 0.04	1.60 ± 0.61	5.50
0.75	0.25 ± 0.08	1.61 ± 0.67	5.16
1.00	0.30 ± 0.11	1.58 ± 0.84	4.20

3.2 Optical bandgap

Bandgap energy of the powders, determined by UV-Vis spectrophotometer, were in the range between 2.46 to 3.01 eV , with the minimum bandgap observed in $\text{Sr}_{0.75}\text{Ca}_{0.25}\text{TiO}_3$. The experimental results revealed that minimization of bandgap energy occurred as a result of doping, as shown in Figure 3. The results from this study were being agreed with studies conducted previously. It has been reported that doping could introduce impurity and generated the allowed energy states in the bandgap, resulting in narrower bandgap [23-24]. According to Bark et al. [25], doping of bismuth by lanthanum and cobalt led to a decrease of bandgap energy from 3.1 eV to 2.5 eV , while Abbas et al. [26] reported reduction of bandgap energy as a result of iron doping in strontium titanate.

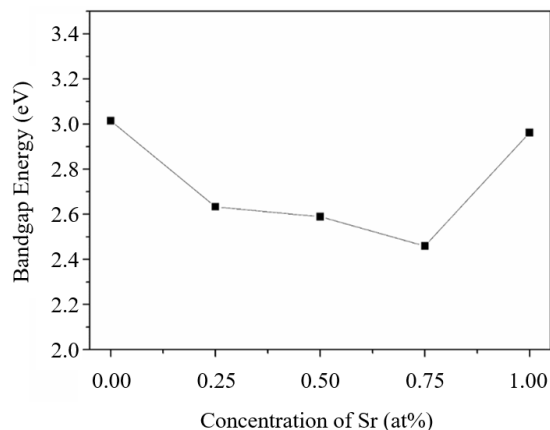


Figure 3. Bandgap energy of $\text{Sr}_x\text{Ca}_{(1-x)}\text{TiO}_3$, where $x=0, 0.25, 0.5, 0.75$ and 1 .

3.3 Photocatalytic activity

Light transmittance of the suspension containing methylene blue and the synthesized powders as well as methylene blue decomposition were conducted to evaluate photocatalytic performance of the powders. Since photocatalytic dye degradation mechanisms

involves electrons, holes, and their interaction with oxygen, hydroxide, water or other reactive species to form reactive radicals capable of decomposing organic dye, materials with outstanding photocatalytic performance tend to exhibit superior degradation ability and high transmittance.

At the wavelength close to 660 nanometers, maximum transmittance of the suspension was observed in $Sr_{0.75}Ca_{0.25}TiO_3$ powders, as shown in Figure 4. In Figure 5, methylene blue degradation as a function of Sr concentrations was demonstrated. The results revealed the greatest methylene blue decomposition and best potential photocatalytic performance in $Sr_{0.75}Ca_{0.25}TiO_3$ powder. Dye decomposition of the $Sr_{0.75}Ca_{0.25}TiO_3$ powder was found to be 43%. While the value was inferior to that of common photocatalysts such as titanium dioxide and zinc oxide, percent methylene blue decomposition of the $Sr_{0.75}Ca_{0.25}TiO_3$ powder was in the same range as that of tin oxide and Er-doped calcium titanate, as shown in Table 2.

Since all of the powder contained particles with comparable sizes and specific surface areas, the highest photocatalytic activity of $Sr_{0.75}Ca_{0.25}TiO_3$ powders was mainly attributed to narrow bandgap energy.

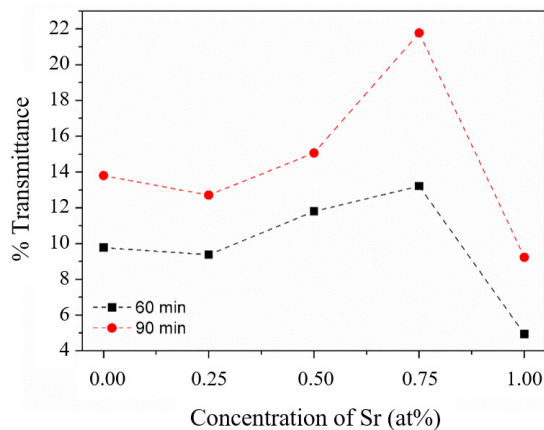


Figure 4. Light transmittance of the suspension containing $Sr_xCa_{(1-x)}TiO_3$, where $x=0, 0.25, 0.5, 0.75$ and 1 , with the measurements conducted at 60 and 90 min after exposing to UV irradiation.

Table 2. A summary of oxide powders for degradation of methylene blue.

Type-oxide	% Degradation (at 60 min)	Reference
TiO_2	72	[27]
ZnO	97	[28]
SnO_2	40	[29]
$CaTiO_3-Er^{3+}$ 1 at%	35	[30]
$Sr_{0.75}Ca_{0.25}TiO_3$	43	Current work

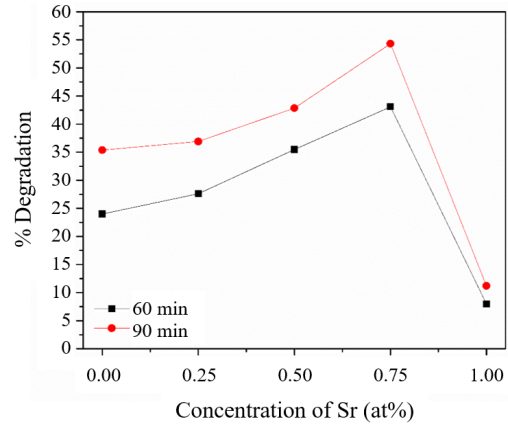


Figure 5. Degradation of methylene blue containing $Sr_xCa_{(1-x)}TiO_3$, where $x=0, 0.25, 0.5, 0.75$ and 1 powder, with the measurements conducted at 60 and 90 min.

3.4 Antibacterial test

Reduction of gram-positive *Staphylococcus aureus* colonies was determined. At the powder concentration of 150 ppm, the number of bacterial colony were reduced, as shown in Figure 6. Percent reduction of bacterial colony was in the range between 91 and 97%. As shown in Table 3, the best and the poorest antibacterial performance were observed in $Sr_{0.75}Ca_{0.25}TiO_3$ and $SrTiO_3$ powders, respectively. The antibacterial activity results agreed well with the photocatalytic performance [31-33].

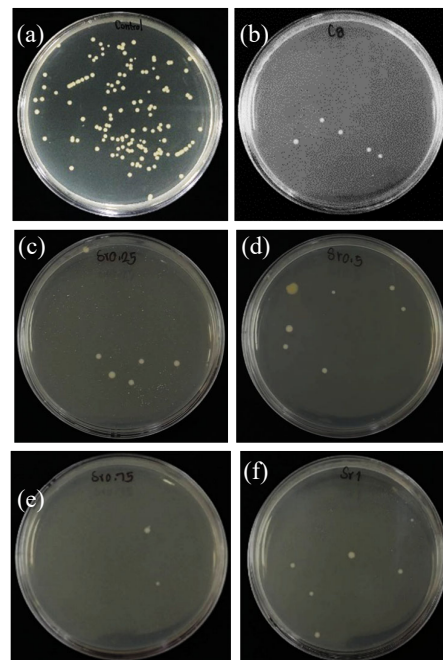


Figure 6. Antibacterial test of powders with compositions: (a) Control-no powder addition, (b) with $CaTiO_3$ powder, (c) with $Sr_{0.25}Ca_{0.75}TiO_3$ powder, (d) with $Sr_{0.5}Ca_{0.5}TiO_3$ powder, (e) with $Sr_{0.75}Ca_{0.25}TiO_3$ powder, and (f) with $SrTiO_3$ powder.

Table 3. Antibacterial activity of Sr_xCa_(1-x)TiO₃.

Concentration of Sr (at%)	Colony reduction (%)
0.00	94.03
0.25	94.02
0.5	94.78
0.75	97.01
1.00	91.04

4. Conclusions

Solution combustion technique was employed in synthesis of Sr_xCa_(1-x)TiO₃ (x = 0, 0.25, 0.5, 0.75 and 1) powders. Single phase CaTiO₃, Sr_xCa_(1-x)TiO₃ and SrTiO₃ powders containing sub-micrometer sized particles were observed. Reduction of bandgap energy occurred in doped powders, with the minimum value of 2.46 eV in Sr_{0.75}Ca_{0.25}TiO₃ powder. Photocatalytic performance, indicated by methylene blue decomposition was improved in doped powders, with the maximum dye degradation in Sr_{0.75}Ca_{0.25}TiO₃ powder. Percent reduction of bacterial colony was in the range between 91 and 97%. Antibacterial performance was being agreed with the photocatalytic performance. Enhancement of photocatalytic degradation of methylene blue and antibacterial activity was mainly attributed to minimal bandgap energy.

5. Acknowledgements

The authors gratefully acknowledge financial support from Kasetsart University Research and Development Institute (KURDI). Equipment supports from the Department of Materials Engineering, Faculty of Engineering, Kasetsart University are gratefully acknowledged.

References

- [1] L. Nanasekaran, R. Hemamalini, R. Saravanan, K. Ravichandran, F. Gracia, and S. Agarwal, "Synthesis and characterization of metal oxides (CeO₂, CuO, NiO, Mn₃O₄, SnO₂ and ZnO) nanoparticles as photo catalysts for degradation of textile dyes," *Journal of Photochemistry and Photobiology B: Biology*, vol. 173, pp. 43-49, 2017.
- [2] J. Qin, C. Yang, M. Cao, X. Zhang, S. Rajendran, and S. Limpanart, "Two-dimensional porous sheet-like carbon-doped ZnO/g-C₃N₄ nanocomposite with high visible-light photocatalytic performance," *Materials Letters*, vol. 189, pp.156-159, 2017.
- [3] R. Saravanan, D. Manoj D, J. Qin, M. Naushad, F. Gracia, and A. F. Lee, "Mechanochemical synthesis of Ag/TiO₂ for photocatalytic methyl orange degradation and hydrogen production," *Process Safety and Environmental Protection*, vol. 120, pp. 339-347, 2018.
- [4] B. Luo, X. Wang, E. Tian, G. Li, and L. Li, "Electronic structure, optical and dielectric properties of BaTiO₃/CaTiO₃/SrTiO₃ ferroelectric superlattices from first-principles calculations," *Journal of Materials Chemistry C*, vol. 3, pp. 8625-8633, 2015.
- [5] O. Jongprateep and N. Sato, "Effects of synthesis techniques on chemical composition, microstructure and dielectric properties of Mg-doped calcium titanate," *AIP Conference Proceedings*, vol. 1957, 2018.
- [6] X. Xiong, R. Tian, X. Lin, D. Chu, and S. Li, "Formation and photocatalytic activity of BaTiO₃ nanocubes via hydrothermal process," *Journal of Nanomaterials*, pp. 12-15, 2015.
- [7] E. Grabowska, "Selected perovskite oxides: Characterization, preparation and photocatalytic properties—A review," *Applied Catalysis B: Environmental*, Vol. 186, pp. 97-126, 2016.
- [8] J. Shi and L. Guo, "ABO₃-based photocatalysts for water splitting," *Progress in Natural Science: Materials International*, vol. 22, no. 6, pp. 592-615, 2012.
- [9] T. Kako, Z. Zou, M. Katagiri, and J. Ye, "Decomposition of organic compounds over NaBiO₃ under visible light irradiation," *Chemistry of Materials*, vol. 19, pp. 198-202, 2016.
- [10] H. Dong, G. Zeng, L. Tang, C. Fan, C. Zhang, and X. He, "An overview on limitations of TiO₂-based particles for photocatalytic degradation of organic pollutants and the corresponding countermeasures," *Water Research*, vol. 79, pp. 128-146, 2015.
- [11] S. S. Arbu, R. R. Hawaldar, S. Varma, S. B. Waghmode, and B. N. Wani, "Synthesis and characterization of ATiO₃ (A =Ca, Sr and Ba) perovskites and their photocatalytic activity under solar irradiation," *Science of Advanced Materials*, vol. 4, pp. 568-572, 2012.
- [12] X. Zhou, J. Shi, and C. Li, "Effect of metal doping on electronic structure and visible light absorption of SrTiO₃ and NaTaO₃ (Metal = Mn, Fe, and Co)," *The Journal of Physical Chemistry C*, vol. 115, no. 16, pp. 8305-8311, 2011.
- [13] J. Y. Han and C. W. Bark, "Tunable band gap of iron-doped lanthanum-modified bismuth titanate synthesized by using the thermal decomposition of a secondary phase," *Journal of the Korean Physical Society*, vol. 66, no.9, pp. 1371-1375, 2015.
- [14] H. Zhang, G. Chen, X. He, and J. Xu, "Electronic structure and photocatalytic properties of Ag-La codoped CaTiO₃," *Journal of Alloys and Compounds*, vol. 516, pp. 91-95, 2012.
- [15] J. Kong, T. Yang, Z. Rui, and H. Ji, "Perovskite-based photocatalysts for organic contaminants

- removal: Current status and future perspectives”, *Catalysis Today* 2018, In press.
- [16] T. Tubchareon, R. Klaysri, and P. Prasertthadam, “A comparison of different A-, A-B-, and B-site incorporated in $(Ba_{0.5}Sr_{0.5})TiO_3$ on photocatalytic application,” *Advances in Optical Technologies*, pp. 1-15, 2015.
- [17] L. F. da Silva, O. F. Lopes, V. R. de Mendonca, K. T. G. Carvalho, E. Longo, C. Ribeiro, and V. R. Mastelaro, “An understanding of the photocatalytic properties and pollutant degradation mechanism of $SrTiO_3$ nanoparticles,” *Photochemistry and Photobiology*, vol. 92, pp. 371-378, 2016.
- [18] T. Kizuki, M. Tomiharu, and T. Kokubo, “Antibacterial and bioactive calcium titanate layers formed on Ti metal and its alloys,” *Journal of Materials Science: Materials in Medicine*, vol. 25, pp. 1737-1746, 2014.
- [19] L. Zhang, P. Y. Tan, C. L. Chow, C. K. Lim, O. K. Tan, M. S. Tse, and C. C. Sze, “Antibacterial activities of mechanochemically synthesized perovskite strontium titanate ferrite metal oxide,” *Colloids and Surfaces A: Physicochemical and Engineering Aspects*, vol. 456, pp. 169-175, 2014.
- [20] S. S. Gaikwad, A. V. Borhade, and V.B. Gaikwad, “A green chemistry approach for synthesis of $CaTiO_3$ photocatalyst: Its effects on degradation of methylene blue, phytotoxicity and microbial study,” *Der Pharma Chemica*, vol. 4, pp. 184-193, 2012.
- [21] M. Romero-Sá ez, L. Y. Jaramillo, R. Saravanan, N. Benito, E. Pabón, E. Mosquera, and F. Gracia, “Notable photocatalytic activity of TiO_2 -polyethylene nanocomposites for visible light degradation of organic pollutants,” *eXPRESS Polymer Letters*, vol. 11, no.11, pp. 899-909, 2017.
- [22] O. Jongprateep, N. Sato, S. Boonsalee, J. H. Pee, “Effects of chemical composition on structure and dielectric constants of $Sr_xCa_{(1-x)}TiO_3$ synthesized by solution combustion technique,” *Materials Today: Proceedings*, vol. 5, pp. 14992-14997, 2018.
- [23] M. C. Wu, W. C. Chen, S. H. Chan and W. F. Su, “The effect of strontium and barium doping on perovskite-structured energy materials for photovoltaic applications,” *Applied Surface Science*, vol. 429, pp. 9-15, 2018.
- [24] M. Pazoki, T. J. Jacobsson, A. Hagfeldt, G. Boschloo, and T. Edvinsson, “Effect of metal cation replacement on the electronic structure of metal organic halide perovskites: replacement of lead with alkaline-earth metals,” *Physical Review B*, vol. 93, 2016.
- [25] C. W. Bark, “Structural and optical properties of bandgap engineered bismuth titanate by cobalt doping,” *Metals and Materials International*, vol. 19, pp. 1361-1364, 2013.
- [26] H. A. Abbas and T. S. Jamil, “Nano sized Fe doped strontium titanate for photocatalytic degradation of dibutyl phthalate under visible light,” *Advanced Materials Letters*, vol. 7, pp. 467-471, 2016.
- [27] L. Gnanasekaran, R. Hemamalini, R. Saravanan, K. Ravichandran, F. Gracia, and V. K. Gupta, “Intermediate state created by dopant ions (Mn, Co and Zr) into TiO_2 nanoparticles for degradation of dyes under visible light,” *Journal of Molecular Liquids*, vol. 223, pp. 652-659, 2016.
- [28] Q. Zhang, M. Xu, B. You, Q. Zhang, H. Yuan, and K. Ostrikov, “Oxygen vacancy-mediated ZnO nanoparticle photocatalyst for degradation of methylene blue,” *Applied Sciences*, vol. 8, pp. 353, 2018.
- [29] S. P. Kim, M. Y. Choi, and H. C. Choi, “Photocatalytic activity of SnO_2 nanoparticles in methylene blue degradation,” *Materials Research Bulletin*, vol. 74, pp. 85-89, 2016.
- [30] L. M. Lozano-Sánchez, S. Obregón, L. A. Díaz-Torres, S. W. Lee, and V. Rodríguez-González, “Visible and near-infrared light-driven photocatalytic activity of erbium-doped $CaTiO_3$ system,” *Journal of Molecular Catalysis A: Chemical*, vol. 410, pp. 19-25, 2015.
- [31] C. Singh, A. Wagle, and M. Rakesh, “Doped $LaCoO_3$ perovskite with Fe: A catalyst with potential antibacterial activity,” *Vacuum*, vol. 146, pp. 468-473, 2017.
- [32] T. Shao-zao, Z. Li-ling, X. Liao-yuan, L. Ying-liang, and L. Du-xin, “Structure and antibacterial activity of new layered perovskite compounds,” *Transactions of Nonferrous Metals Society of China*, vol. 17, pp. 257-261, 2007.
- [33] S. Raja, D. Bheeman, R. Rajamani, S. Pattiyappan, S. Sugamaram, and C. S. Bellan, “Synthesis, characterization and remedial aspect of $BaTiO_3$ nanoparticles against bacteria,” *Nanomedicine and Nanobiology*, vol. 1, pp. 1-5, 2014.